

Article

Petrogenesis of the Late Carboniferous Trondhjemite in Central Inner Mongolia in North China and Constraints of Intra-Oceanic Subduction in the Southern Paleo-Asian Ocean

Peipei Dong ^{1,2}, Yingjie Li ^{1,2,*}, Yan Xie ³, Jinfang Wang ¹ and Hongyang Li ¹¹ College of Earth Sciences, Hebei GEO University, Shijiazhuang 050031, China² Hebei Key Laboratory of Strategic Critical Mineral Resources, Hebei GEO University, Shijiazhuang 050031, China³ Inner Mongolia Mining Exploitation Co., Ltd., Hohhot 010020, China

* Correspondence: liyingjie820@126.com; Tel.: +86-15632364069

Abstract: Intra-oceanic subduction is a fundamental process on Earth, the study of which can improve the understanding of plate tectonic processes and the history of continental growth. Here, we report on newly recognized trondhjemite in the north of Diyanmiao ophiolite belt in North China. The trondhjemite was found along the Erenhot-Hegenshan suture zone. U-Pb zircon dating revealed that the trondhjemite crystallized at 309 ± 2.1 Ma. The trondhjemite had a high amount of SiO₂ (68.94–76.45 wt %), Al₂O₃ (13.37–15.90 wt %), and Sr (232–601 ppm); and a low amount of K₂O (1.57–2.70 wt %), Y (6.91–9.39 ppm), Ni (1.10–4.19 ppm), and Cr (1.55–13.50 ppm). The Na₂O/K₂O ratios were 1.90–4.37. There was a lack of negative Eu anomalies. It was relatively enriched in large-ion lithophile elements (LILEs) such as Rb, Ba, K, and Sr; was depleted in high-field-strength elements (HFSEs) such as Nb, Ta, Ti, and P; and had low total rare-earth element (REE) contents (27.73–49.63 ppm) with distinct REE fractionation (chondrite-normalized (La/Yb)_N of 5.76–10.52), which was similar to adakitic rocks formed by partial melting of subducted oceanic crust. The trondhjemite, together with Diyanmiao ophiolite (335.6 Ma), may have formed during the stages of intra-oceanic subduction, suggesting that in the Early Carboniferous–Late Carboniferous, the southern Paleo-Asian Ocean was in its subduction stage.

Keywords: trondhjemite; ophiolite; intra-oceanic subduction; late Carboniferous; Paleo-Asian Ocean; Inner Mongolia



Citation: Dong, P.; Li, Y.; Xie, Y.; Wang, J.; Li, H. Petrogenesis of the Late Carboniferous Trondhjemite in Central Inner Mongolia in North China and Constraints of Intra-Oceanic Subduction in the Southern Paleo-Asian Ocean. *Minerals* **2022**, *12*, 1212. <https://doi.org/10.3390/min12101212>

Academic Editor: Delphine Bosch

Received: 6 July 2022

Accepted: 21 September 2022

Published: 26 September 2022

Publisher's Note: MDPI stays neutral with regard to jurisdictional claims in published maps and institutional affiliations.



Copyright: © 2022 by the authors. Licensee MDPI, Basel, Switzerland. This article is an open access article distributed under the terms and conditions of the Creative Commons Attribution (CC BY) license (<https://creativecommons.org/licenses/by/4.0/>).

1. Introduction

Tonalite–trondhjemite–granodiorite (TTG) suites have always been one of the important subjects in the field of geology [1,2]. As an important component of the crust, Tonalite–trondhjemite–granodiorite (TTG) rocks are not only widely distributed in the Archean Paleoproterozoic granite greenstone belt, but also an important part of the Phanerozoic accretionary orogenic belt (the oceanic subduction belt). Geochemical and experimental petrological studies have confirmed that TTG suites were formed by partial melting of water-bearing basaltic rocks in garnet amphibolite facies or eclogite facies [2,3]. It is generally believed that the Phanerozoic TTG suites are a typical igneous tectonic assemblage formed in the island arc environment of the oceanic subduction zone and were the product of dehydration and melting of oceanic subduction basalt slabs [1,4,5]. This is an important rock record of crustal accretion and tectonic evolution in orogenic belts. The study showed that the Phanerozoic TTG magmatism was an important geological process for the growth of the Cenozoic continental crust. A tonalite–trondhjemite–granodiorite (TTG) assemblage represents a growth event of the Cenozoic continental crust or accretion of the continental crust, which is of great significance in the formation of the continental prototype and is also the key to characterizing the accretion of the Phanerozoic accretionary orogenic belt

and the ocean continent transition [6,7]. Therefore, a study on the petrogenesis, tectonic environment, and formation age of TTGs can provide important petrological, chronological, and geochemical bases for the formation, accretionary mechanism, and tectonic evolution of an new continental crust.

The Central Asian Orogenic Belt (CAOB) is located between the Siberian plate and the Tarim and North China plates (Figure 1a). The CAOB is one of the Earth's largest accretionary orogens and records a complex history of subduction and collision episodes pertaining to the Neoproterozoic–Paleozoic closure of the Paleo-Asian Ocean (PAO) [8,9]. Its prolonged, episodic, diachronous, and mostly Paleozoic tectonic evolution is characterized by accretion of a diverse array of terranes including continental-margin fragments, seamounts, fore-arc and back-arc basins, and oceanic arcs [10–18]. The archipelago-type southwestern Pacific oceanic is often regarded as a modern tectonic analog [10,14,19]. It is considered to be a typical accretionary orogenic belt (Figure 1b) [19–21]. However, the closing time and location of the Paleozoic Paleo-Asian Ocean in the eastern part of the CAOB is still obviously controversial. Xiao et al. [22] and Jian et al. [23] considered that the Paleo-Asian Ocean was in the ocean continent transition stage in the Carboniferous–Permian and closed along the Solonker–Xilamulun suture in the Late Permian–Early Triassic. Another view is that the Paleo-Asian Ocean closed in the middle-late Devonian and the late Paleozoic igneous rocks were formed in an intracontinental rifting setting [24]. The main reason for the inconsistency is that there is no unified understanding of the reconstruction of the paleo-ocean basin, the late Paleozoic tectonic magmatic process, and its geotectonic background. There is a lack of systematic identification and research from the ophiolite to the initial subduction intra-oceanic arc [20]. Recent studies on the Izu–Bonin–Mariana (IBM) forearc revealed that the SSZ type ophiolite and forearc rock assemblages were first formed during the initial subduction [25]. Therefore, identifying and studying the spatiotemporal distribution and internal genetic relationship between island arc magmatic rocks and SSZ ophiolites can deepen the understanding of the subduction and extinction process of the Paleo-Asian Ocean.

The southeastern CAOB contains several sub-parallel ophiolite belts with variable ages [26] (Figure 1b). The Hegenshan ophiolite–arc–accretionary belt is located in the northern of the southeastern CAOB (Figure 1b). The Hegenshan suture zone is widely distributed with Paleozoic ophiolites (belts) and subducted island-arc magmatic rocks, especially the Early Carboniferous–Late Carboniferous ophiolites and Early Carboniferous–Early Permian island-arc magmatic rocks. Most previous studies considered that the Hegenshan ophiolites were formed in a mid-ocean ridge environment [27,28], and some scholars also believed that the Hegenshan ophiolites have the characteristics of a subduction zone, such as an island arc-marginal basin system or back arc extensional ocean basin [29], but lacking systematic identification of an intra-ocean arc [21].

Recent studies have shown that some ophiolites in the Hegenshan ophiolite–arc–accretionary belt were formed in an intra-oceanic forearc setting, such as Diyanmiao ophiolite [30] and Meilaotewula ophiolite [31]. Therefore, the recognition of intra-oceanic arcs in SSZ-type ophiolites is an effective method to understand the process of intra-oceanic subduction and subsequent orogenesis [32].

Our regional geological mapping revealed the occurrence of Late Carboniferous trondhjemite in the north of the Diyanmiao SSZ-type ophiolite zone (Figure 2), providing an opportunity for a systematic study of intra-oceanic subduction of the southeastern part of the Paleo-Asian Ocean (PAO). Fore-arc basalt, boninitic rocks, and adakites indicated that the Diyanmiao ophiolite formed in the incipient forearc of suprasubduction zone [21,32]. The newly discovered Gaolihan trondhjemite provides new information for the systematic study of intra-oceanic subduction in the southern PAO. Here, we present the field relations, petrography, major and trace-element geochemistry, and zircon U–Pb geochronology of this trondhjemite. We provide clear evidence for a progressively evolving of an intra-oceanic arc and intra-oceanic subduction in the Late Carboniferous.

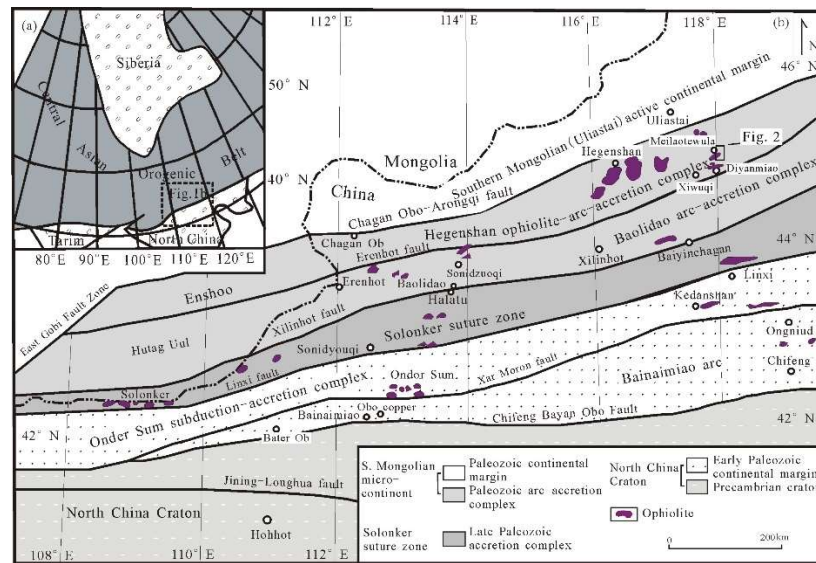


Figure 1. (a) Tectonic framework of the North China–Mongolia segment of the Central Asian Orogenic Belt [16]. (b) Geological sketch map of the northern China–Mongolia tract [17,18].

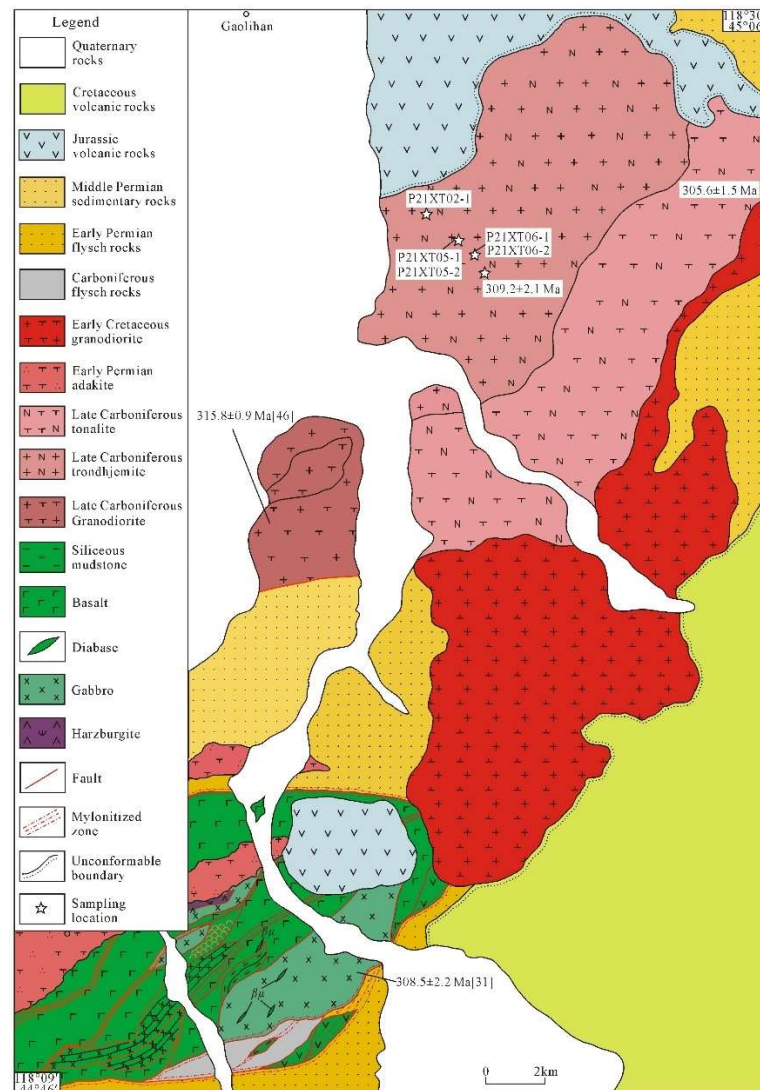


Figure 2. Geological map of the Gaolihan trondhjemite.

2. Geological Setting

The southern CAOBS extends from southern Mongolia via Inner Mongolia to the Great Xing'an Range [21,33]. This region has been subdivided into three tectonic zones, the southern subduction–accretionary orogen, the Solonker suture zone, and the northern subduction–accretionary orogen. [22,34] (Figure 1b).

The Hegenshan ophiolite-arc-accretionary complex extends ~500 km from Erenhot to the Hegenshan Mountains in the northeast [30]. This complex is sandwiched between the Chagan Obo–Arongqi and Erenhot faults and contains the Erenhot ophiolitic complex, Hegenshan ophiolite, and Meilaotewula and Diyanmiao ophiolites [31,32]. The Erenhot–Hegenshan fault zone contains abundant Early Carboniferous to Late Carboniferous SSZ-type ophiolites and Late Carboniferous to Early Permian island arc magmatic rocks. In these island arc magmatic rocks, geologists [35,36] have continuously identified TTG rocks. These island arc magmatic rocks, particularly the arc crust or continental crust formed by the tectonic combination of intra-oceanic arc or intra-oceanic arc igneous rocks, record the information of ocean land-transformation processes such as subduction of the Paleo-Asian ocean crust, TTG magmatism, and growth of the new continental crust. Therefore, this paper attempted to provide constraints for the subduction and extinction process of the Paleo-Asian Ocean and the growth of the Cenozoic continental crust tectonic magmatic events through a detailed study of the petrology, geochemistry, and zircon U-Pb chronology of the Gaolihan trondhjemite, which is closely related to the Diyanmiao intra-oceanic arc.

3. Field Relationship and Petrography

The newly recognized Gaolihan trondhjemite is located in the north of Diyanmiao area (Figure 2) ($118^{\circ}21'$, $45^{\circ}01'$). The trondhjemite is discordantly overlain by Jurassic intermediate volcanic rocks and are intruded by Late Carboniferous tonalite (Figure 2). The Diyanmiao SSZ ophiolite is in faulted contact with Early Permian marine flysch deposits [21] (Figure 2), which comprise mainly, from bottom to top, harzburgite, layered-massive gabbro, diabase veins, fore-arc basalts (FAB), boninite, chert, and siliceous mudstone [21], a lithological assemblage that is similar to the SSZ-ophiolite-type sequence of the IBM system [37]. Most units of the ophiolite and its related rocks were subjected to mylonitization (Figure 2).

The Gaolihan trondhjemite is greyish-white to grey in color and medium- to coarse-grained (Figure 3a–d). It contains mainly plagioclase (60–65%), quartz (25–30%), and biotite (5–10%). The oligoclase occurs as euhedral to subhedral grains. The composition of the plagioclase is sodic oligoclase with $An = 10$ –15 based on extinction angle measurements. The plagioclase is typically partially sericitized. The quartz is xenomorphic granular. The biotite is commonly altered to chlorite.

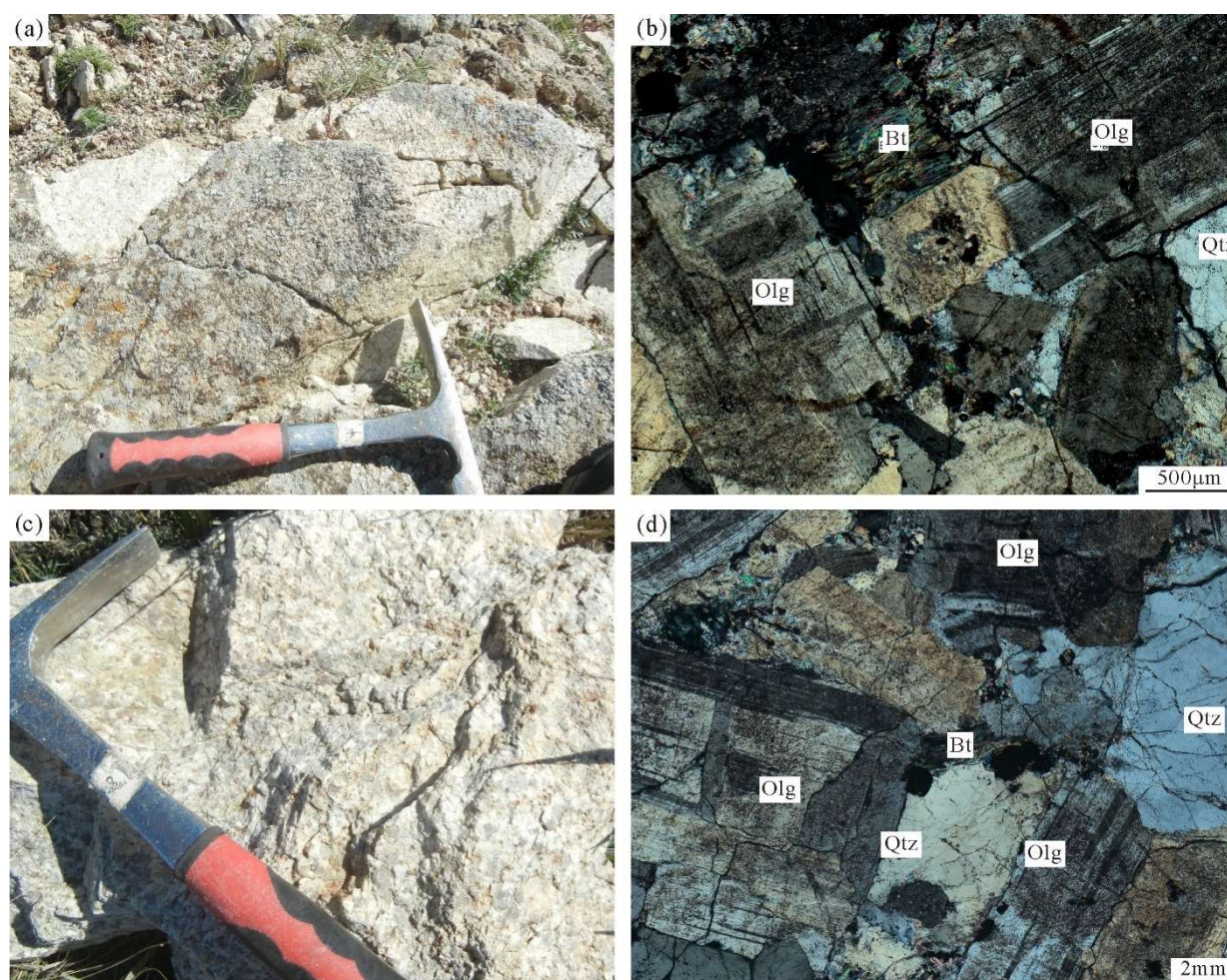


Figure 3. Field occurrences (a,c) and photomicrographs (b,d) of the Gaolihan trondhjemite. (a) Field occurrence of the fine-medium-grained trondhjemite. (b) Characteristic fine-medium-grained subhedral granular texture of the trondhjemite. (c) Field occurrence of the coarse-grained trondhjemite. (d) Photomicrograph of the trondhjemite. Olg—oligoclase; Qtz—quartz; Bt—biotite.

4. Analytical Methods

The whole-rock geochemical and zircon U-Pb isotopic analyses were undertaken at the Wuhan Sample Solution Analytical Technology Co., Ltd, Wuhan, China.

A Zsx Primus II wavelength dispersive X-ray fluorescence spectrometer (XRF) produced by RIGAKU, Japan, was used for the analysis of major elements in the whole rock; the X-ray tube was a 4.0 Kw end window Rh target. All major element analysis lines were $k\alpha$ and the standard curve used the national standard material: the rock standard sample GBW07101-14. The relative standard deviation (RSD) was less than 2%.

Trace-element analyses of whole rock were conducted on an Agilent 7700e ICP-MS at the Wuhan Sample Solution Analytical Technology Co., Ltd., Wuhan, China. The detailed sample-digesting procedure was as follows: (1) Sample powder (200 mesh) was placed in an oven at 105 °C for drying for 12 h; (2) 50 mg of sample powder was accurately weighed and placed in a Teflon bomb; (3) 1 mL of HNO₃ and 1 mL of HF were slowly added into the Teflon bomb; (4) the Teflon bomb was enclosed in a stainless steel pressure jacket and heated to 190 °C in an oven for >24 h; (5) after cooling, the Teflon bomb was opened and placed on a hotplate at 140 °C and evaporated to incipient dryness, and then 1 mL HNO₃ was added and evaporated to dryness again; (6) 1 mL of HNO₃, 1 mL of MQ water, and 1 mL of internal standard solution at 1 ppm In were added, and the Teflon bomb was resealed and placed in the oven at 190 °C for >12 h; (7) the final solution was transferred to a polyethylene bottle and diluted to 100 g via the addition of 2% HNO₃.

Zircons were separated using standard density and magnetic techniques and then handpicked under a binocular microscope. Grains were then imaged using cathodoluminescence (CL) to characterize their internal morphologies. Zircon 91,500 and glass NIST610 were used as external standards for U-Pb dating and trace-element calibration, respectively. The Excel-based software ICPMSDataCal was used to perform off-line selection and integration of the background and analyzed signals, time-drift correction, and quantitative calibration for the trace-element analysis and U-Pb dating [38]. Concordia diagrams and weighted mean calculations were made using Isoplot/Ex_ver3 (Berkeley CA, USA, Kenneth R. Ludwig, 2003) [39].

5. Analytical Results

5.1. Major and Trace-Element Analyses

The loss-on-ignition (LOI) contents of the Gaolihan trondhjemite was 1.06–1.69% (Table 1 [6,35,36,40,41]), which was consistent with petrographic evidence for partial alteration. Furthermore, elements such as Li, Rb, Cs, K, U, and P may be mobile in rocks during hydrothermal alteration [42]. Therefore, in the following discussions, the major element contents were normalized to 100 wt % on an anhydrous basis and we considered some relatively immobile elements (such as high field strength elements: Th, Zr, Hf, Nb, Ta, Ti, and rare-earth elements) for interpretation of the trace-element chemistry.

The Gaolihan trondhjemite samples had high SiO₂ (68.94–72.58 wt %) and Al₂O₃ (14.85–15.90 wt %) contents and low MgO (0.76–1.33 wt %), TiO₂ (0.27–0.52 wt %), and P₂O₅ (0.09–0.14 wt %) contents. The rocks had relatively low concentrations of K₂O (1.37–2.70 wt %) but were enriched in Na₂O (4.80–5.99 wt %); the Na₂O/K₂O ratios were 1.88–4.38 (Table 1). In an An-Ab-Or diagram (Figure 4a), all of the five trondhjemite samples fell into the field of trondhjemite. In a K-Na-Ca diagram (Figure 4b), the trondhjemite samples fell into the field of Archaean TTGs or at the boundary. In a SiO₂ vs. Na₂O + K₂O (TAS) diagram, three trondhjemite samples fell into the field of granodiorite, with two plotting at the quartz monzonite field (Figure 5a). On a K₂O vs. SiO₂ diagram (Figure 5b), the five trondhjemite samples plotted within the calc-alkaline field.

Table 1. Major and trace-element data for the Gaolihan trondhjemite.

Sample	P21XT02-1	P21XT05-1	P21XT05-2	P16XT06-1	P16XT06-2	Phanerozoic TTG	TTG Rock in the Central Asian Orogenic Belt					Late Carboniferous Tonalite	
Major element (wt %) ^a													
SiO ₂	72.58	68.94	69.24	71.81	71.30	65.90	69.05	69.20	64.46	77.17	71.10	66.58	66.45
TiO ₂	0.12	0.44	0.52	0.25	0.27	0.47	0.30	0.31	0.65	0.23	0.45	0.50	0.49
Al ₂ O ₃	15.55	15.90	15.83	14.85	15.23	16.50	13.87	13.19	15.72	11.23	13.85	15.57	16.14
TFe ₂ O ₃	1.24	3.17	3.38	2.01	2.05					1.56	3.41		
MnO	0.06	0.05	0.05	0.06	0.05	0.09	0.09	0.08	0.11	0.14	0.04	0.07	0.07
MgO	0.36	1.24	1.33	0.76	0.77	1.67	1.11	1.25	2.20	0.56	1.17	1.64	1.94
CaO	1.11	0.78	0.56	1.54	1.32	4.36	3.72	2.37	4.82	2.56	2.58	3.39	2.90
Na ₂ O	5.73	5.91	5.99	4.80	5.13	4.00	4.08	4.11	3.65	3.84	3.78	4.25	4.45
K ₂ O	2.08	1.57	1.37	2.55	2.70	2.14	1.65	2.78	1.72	0.89	1.44	1.91	1.81
P ₂ O ₅	0.05	0.14	0.14	0.09	0.09	0.12	0.09	0.08	0.21	0.04	0.15	0.15	0.16
Total ^b	99.94	99.83	99.94	99.80	100.05		97.9	98.35	99.67	100.09	99.97	99.83	99.88
LOI	1.06	1.69	1.55	1.08	1.14							2.11	1.95
Mg [#]	40.34	47.62	47.73	46.92	46.71					41.79		46	51
Trace element (ppm)													
Rb	38.50	32.60	28.10	48.60	53.10	63.00	30.02	50.94	59.50	6.83	57.42	39.80	25.70
Cr	1.55	4.94	5.42	3.93	3.83	32.00	3.48	3.90	9.88	2.85	3.01	11.50	12.30
Co	1.26	6.40	7.15	3.58	3.64	40.70	4.51	6.00	13.5	1.62	6.65	10.60	9.30
Ni	1.10	4.19	5.74	2.82	2.33	12.00	2.65	2.03	5.14	3.07	4.00	6.20	5.90

Table 1. Cont.

Sample	P21XT02-1	P21XT05-1	P21XT05-2	P16XT06-1	P16XT06-2	Phanerozoic TTG	TTG Rock in the Central Asian Orogenic Belt					Late Carboniferous Tonalite	
Sc	1.67	5.41	5.85	3.61	4.00	34.90	7.16	7.16				7.88	6.12
V	11.40	62.00	62.50	34.70	36.70	243.00	75.94	79.10		13.56		90.50	67.50
Zr	68.10	87.90	92.40	84.10	82.00	122.00	118.60	96.84	156.00	45.86	168.37	113.20	99.40
Hf	2.04	2.68	2.96	2.47	2.56	3.40	3.61	3.22	4.28	1.37	4.18	7.00	7.52
Ta	0.19	0.18	0.23	0.18	0.18	0.75	0.19	0.19	0.44	0.03	0.17	0.20	0.23
Sr	286.00	601.00	586.00	439.00	412.00	493.00	207.60	143.74	336.00	71.82	293.56	458.60	421.20
Ba	426.00	527.00	452.00	427.00	432.00	716.00	354.80	444.20	359.00	59.77	394.60	528.20	413.20
Nb	2.17	2.89	3.51	1.91	2.19	6.70	2.21	2.22	6.27	0.33	3.16	2.78	2.93
Cs	0.79	2.38	2.04	1.09	0.96		0.44	0.81	3.76				
Ga	17.10	17.80	17.50	18.30	18.20		14.37	15.94					
Th	0.91	3.90	4.62	3.00	3.07	7.60	2.97	3.26	4.78	0.59	5.09	4.29	3.73
U	0.31	0.83	0.85	0.80	0.91	1.90	0.73	3.47	1.04	0.16	2.09	1.04	0.95
La	6.48	14.30	16.20	8.10	10.80	17.00	5.69	7.19	17.80	7.44	17.48	10.89	12.67
Ce	13.90	30.70	36.80	18.70	23.10	34.00	13.31	14.42	36.20	21.13	35.16	21.62	27.35
Pr	1.73	3.59	4.32	2.41	2.78		1.75	2.04	4.70	2.50	3.22	2.73	3.13
Nd	6.68	14.00	16.30	9.25	10.70	16.00	7.90	8.74	19.20	10.02	11.54	10.90	13.58
Sm	1.42	2.62	3.23	1.83	2.09	3.10	2.18	2.24	4.06	2.61	1.92	2.16	2.35
Eu	0.40	0.79	0.89	0.56	0.59	0.84	0.71	0.68	1.10	0.47	0.62	0.74	0.83
Gd	1.30	2.10	2.42	1.50	1.56	2.80	2.60	2.54	4.44	2.56	1.94	1.83	1.99
Tb	0.24	0.31	0.37	0.21	0.23	0.40	0.44	0.41	0.62		0.25	0.30	0.32
Dy	1.25	1.62	1.87	1.14	1.39		3.28	2.94	3.86	3.09	1.37	1.71	1.82
Ho	0.25	0.31	0.39	0.22	0.25		0.66	0.58	0.80	0.66	0.27	0.31	0.35
Er	0.75	0.86	1.04	0.72	0.74		2.27	2.00	2.26	1.97	0.78	0.89	1.12
Tm	0.12	0.14	0.16	0.11	0.11		0.34	0.30	0.35	0.31	0.10	0.14	0.18
Yb	0.81	0.98	1.16	0.79	0.82	1.16	2.64	2.40	2.54	2.19	0.70	0.91	1.05
Lu	0.12	0.16	0.19	0.14	0.15	0.18	0.40	0.36	0.36	0.35	0.12	0.13	0.18
Y	7.84	9.39	11.1	7.12	7.90	14.50	17.04	14.69	20.10	20.54	7.66	7.86	8.84
Total REE	35.43	72.51	85.41	45.74	55.33		44.17	46.83	98.29	55.73	75.47	55.26	66.89
LREE	30.58	66.04	77.80	40.91	50.08								
HREE	4.85	6.47	7.61	4.83	5.25								
LREE/HREE	6.31	10.20	10.23	8.47	9.54								
(La/Yb) _N	5.76	10.52	9.97	7.34	9.49								
δEu	0.91	1.03	0.98	1.03	1.00		0.91	0.87			0.99		

^a All oxide contents in the samples were recalculated to 100% on a volatile-free basis; ^b total before normalization. ¹Fe₂O₃ as total Fe₂O₃. (La/Yb)_N is ratio of La and Yb normalized by chondrite. Mg[#] = 100 × [Molar Mg/(Mg+Fe²⁺)]. Phanerozoic TTG data from Condie [6]. TTG rock data in the Central Asian Orogenic Belt from [35,36,40]; Late Carboniferous tonalite data from Wang et al., 2021 [41].

The samples had low total rare-earth element (REE) contents (30.58–77.80 ppm) and showed light rare-earth element (LREE) enrichment and heavy rare-earth element (HREE) depletion in the chondrite-normalized REE diagrams ([La/Yb]_N = 5.76–10.52) with no pronounced Eu anomaly (Eu/Eu* = 0.89–1.00; average = 0.96) (Figure 6a). The striking chemical characteristics were the high contents of Sr (286–601 ppm; average = 465 ppm) and low contents of Y (7.12–11.10 ppm; average = 8.66 ppm) and Yb (0.81–1.16 ppm; average = 0.91 ppm); the Sr/Y ratios were 36.48–64.00. The samples had relatively low abundances of compatible elements such as Cr (1.55–5.42 ppm) and Ni (1.10–5.74 ppm). In addition, the samples displayed a relative enrichment in large-ion lithophile elements (LILEs) such as Rb, Ba, K, and Sr; and depletion in high-field-strength elements (HFSEs) such as Nb, Ta, Ti, and P (Figure 6b), showing the trace-element composition characteristics of the island arc magmatic rocks in the oceanic subduction zone [36].

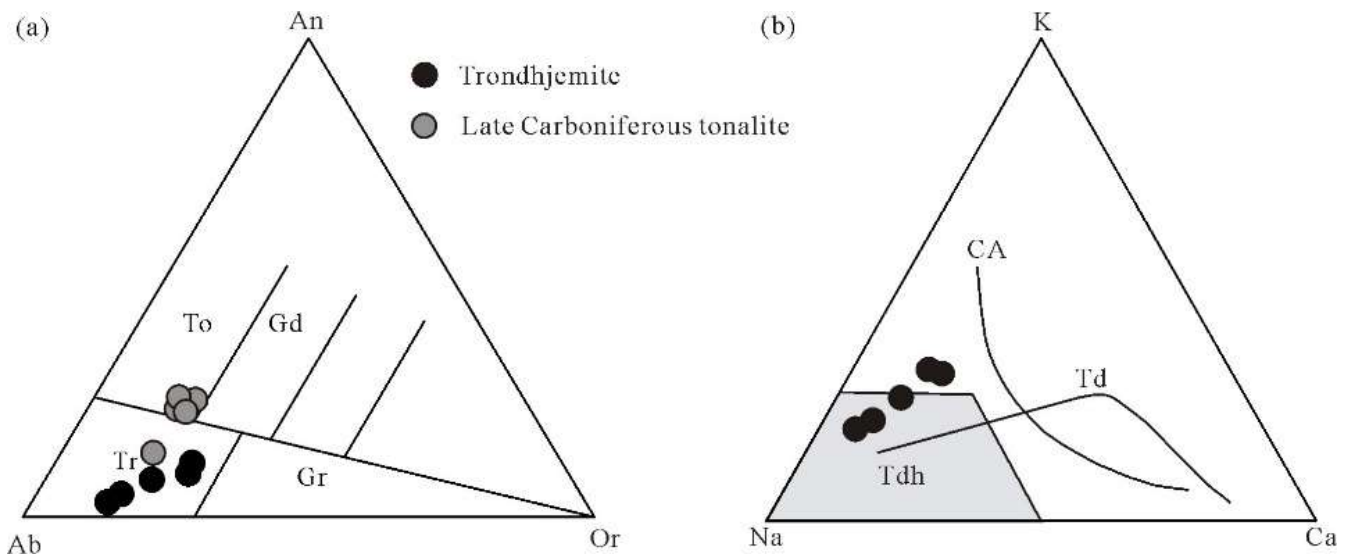


Figure 4. (a) Normative An-Ab-Or triangle [43]; (b) K-Na-Ca triangle [44]. Late Carboniferous tonalite data from Wang et al., 2021 [41]. To = tonalite; Gd = granodiorite; Tr = trondhjemite; Gr = granite; Td = trondhjemitic differentiation trend; CA = classical calc-alkaline trend characterized by K-enrichment during differentiation.

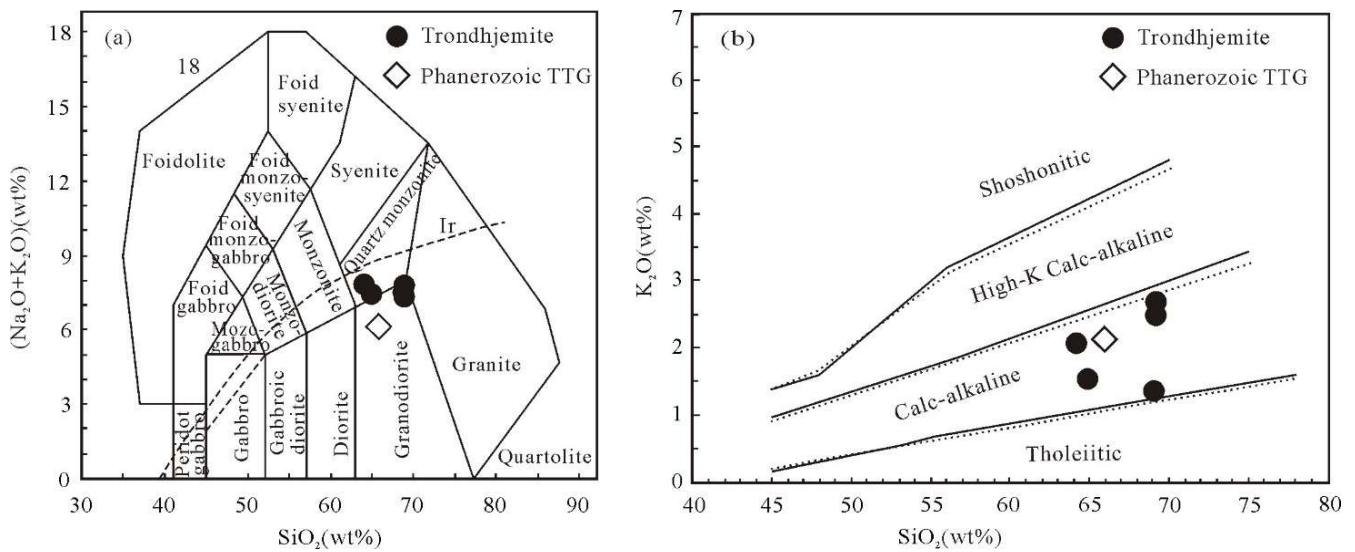


Figure 5. (a) SiO₂ vs. (K₂O + Na₂O) for trondhjemite [45]; (b) SiO₂ vs. K₂O for the Gaolihan trondhjemite [46]. Phanerozoic TTG data are from Condie [6].

Figure 6 [6,40,41,47,48] shows that the trace-element patterns of the Gaolihan trondhjemite were consistent with those of Phanerozoic TTG, adakites within the Diyanmiao SSZ-type ophiolite, and Late Carboniferous tonalite, displaying enrichment in LILEs (K, Rb, and Sr) and depletion in HFSEs (Nb, Ta, and Ti), which was consistent with the island arc and oceanic subduction background [49,50].

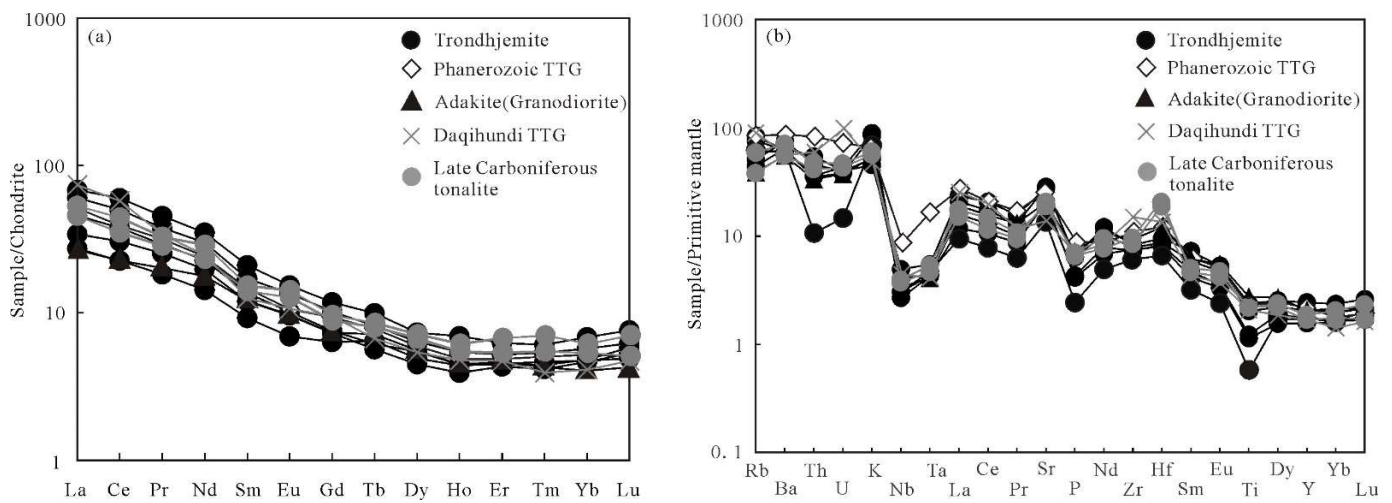


Figure 6. (a) Chondrite-normalized REE distribution patterns and (b) primitive mantle-normalized trace-element diagram for the Gaolihan trondhjemite. The normalizing values are from Sun and McDonough [47]. Phanerozoic TTG data from Condie [6]; adakite (granodiorite) data from Wang et al., 2020 [48]; Daqihundi TTG data from Fan 2020 [40]; Late Carboniferous tonalite data from Wang et al., 2021 [41].

5.2. U-Pb Zircon Ages

The results of the zircon LA-ICP-MS U-Pb dating are summarized in Table 2. Zircon grains separated from this sample (P16TW08) showed an intact crystal shape and subhedral to euhedral morphologies. All analyzed zircon grains were transparent and had oscillatory zoning and broad magmatic zoning in cathodoluminescence (CL) images (Figure 7a). The zircon grains showed relatively narrow, clear, and dense oscillatory zoning with no evidence of resorption or inherited cores; all zircon grains had high Th/U ratios (Table 2), which was characteristic of crystallization from acidic magma [51]. A total of 16 analyses of zircons from sample P16TW08 yielded concordant results with ²⁰⁶Pb/²³⁸U ages ranging from 301 ± 4 to 316 ± 5 Ma. These data yielded a weighted mean age of 309.2 ± 2.1 Ma (MSWD = 0.77) (Figure 7b,c), reflecting the crystallization age of the Gaolihan trondhjemite.

Table 2. LA-ICP-MS zircon U-Pb isotopic analysis of the Gaolihan trondhjemite.

Spot No.	Element (ppm)		Th/U	Isotopic Ratios						Apparent Age (Ma)					
	Th	U		²⁰⁶ Pb/ ²³⁸ U	1σ	²⁰⁷ Pb/ ²³⁵ U	1σ	²⁰⁷ Pb/ ²⁰⁶ Pb	1σ	²⁰⁶ Pb/ ²³⁸ U	1σ	²⁰⁷ Pb/ ²³⁵ U	1σ	²⁰⁷ Pb/ ²⁰⁶ Pb	1σ
P16TW08 Trondhjemite															
01	77	125	0.62	0.0479	0.0007	0.3585	0.0206	0.0540	0.0030	301	4	311	15	369	131
02	47	94	0.50	0.0497	0.0008	0.3580	0.0224	0.0525	0.0035	313	5	311	17	309	152
03	98	146	0.67	0.0488	0.0006	0.3396	0.0164	0.0505	0.0025	307	4	297	12	217	115
04	104	161	0.64	0.0493	0.0007	0.3465	0.0174	0.0514	0.0027	310	4	302	13	257	86
05	83	127	0.65	0.0483	0.0007	0.3509	0.0191	0.0535	0.0029	304	4	305	14	350	131
06	48	97	0.50	0.0498	0.0009	0.3682	0.0228	0.0536	0.0034	313	5	318	17	367	144
07	49	99	0.49	0.0492	0.0008	0.3192	0.0190	0.0480	0.0030	310	5	281	15	98.2	141
08	71	121	0.59	0.0499	0.0007	0.3395	0.0192	0.0494	0.0028	314	4	297	15	165	131
09	50	98	0.51	0.0492	0.0008	0.3740	0.0216	0.0561	0.0035	309	5	323	16	457	134
10	92	131	0.70	0.0486	0.0007	0.3323	0.0168	0.0502	0.0028	306	4	291	13	206	127
11	100	138	0.72	0.0496	0.0007	0.3461	0.0170	0.0512	0.0027	312	4	302	13	250	122
12	339	241	1.41	0.0488	0.0005	0.3305	0.0136	0.0489	0.0020	307	3	290	10	143	94
13	38	79	0.48	0.0488	0.0009	0.3311	0.0220	0.0496	0.0039	307	5	290	17	176	174
14	68	108	0.63	0.0496	0.0007	0.3878	0.0203	0.0571	0.0031	312	5	333	15	494	122
15	53	106	0.50	0.0503	0.0008	0.3486	0.0217	0.0501	0.0033	316	5	304	16	198	156
16	67	118	0.56	0.0494	0.0007	0.3640	0.0200	0.0536	0.0032	311	4	315	15	354	133

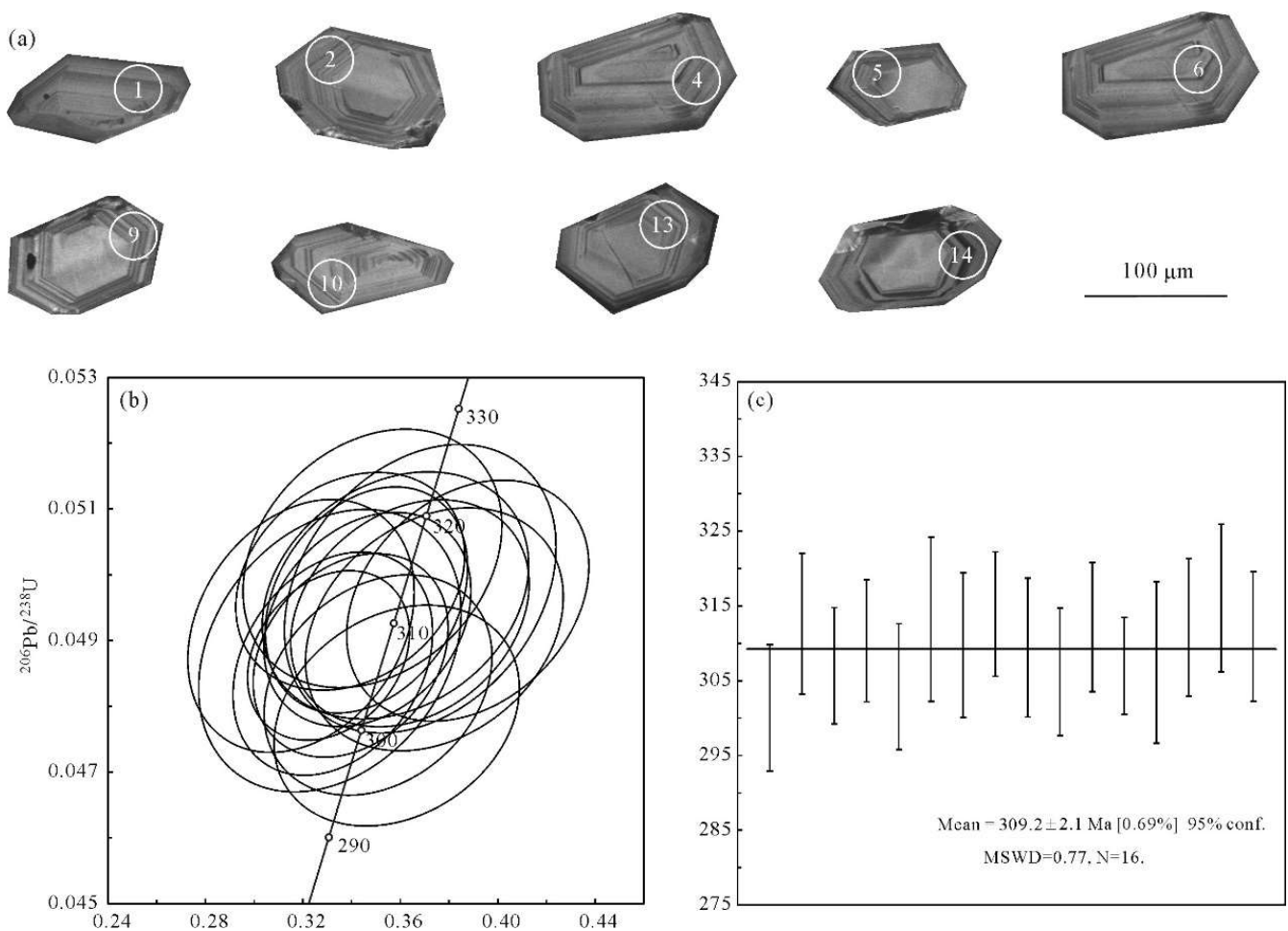


Figure 7. (a) Representative zircon CL images, (b) Concordia curves, and (c) weighted mean age of LA-ICP-MS U-Pb data for the Gaolihan trondhjemite.

6. Discussion

6.1. Petrogenesis of the Trondhjemite

The Gaolihan trondhjemite was characterized by high concentrations of SiO_2 , Al_2O_3 , Na_2O , and Sr, with high Sr/Y ratios (average = 53.44 > 40) but low MgO, Y, and Yb. They were also enriched in LREEs but had low total HREE contents and no clear Eu anomalies (Figure 6a; Table 1), all of which were similar to classic adakite and TTG rocks (Figure 6) and showed a trondhjemitic differentiation trend (Figure 4b). The Gaolihan trondhjemite was high in LREEs and low in HREEs without negative Eu anomalies ($\text{Eu}/\text{Eu}^* = 0.91\text{--}1.03$) that were similar to the REE patterns of Phanerozoic TTG and TTG rock data published in the CAOB [52] (Figure 6a). All samples were enriched in large-ion lithophile elements (LILEs) such as Ba, K, Rb, and Sr; were depleted in high-field-strength elements (HFSEs) such as Nb, Ta, P, and Ti; and were similar to the primitive mantle (PM)-normalized spider-diagram patterns of Phanerozoic TTG [6] (Figure 6b). Furthermore, the Gaolihan trondhjemite showed a trondhjemitic differentiation trend [7,44] as the evolution of Na-rich magmas (Figure 5b). Therefore, through the comparison of petrological characteristics and geochemical characteristics with Phanerozoic TTG and TTG rock data published in the CAOB (Table 2); and by referring to the An-Ab-Or diagram (Figure 4a), K-Na-Ca diagram (Figure 4b), rare-earth-element patterns (Figure 6a), and trace-element diagram (Figure 6b) of the Late Carboniferous tonalite, the Gaolihan trondhjemite may belong to TTG rocks [5].

The basalt melting experiment inferred that TTG-like trondhjemite melts can only be produced when there is free water in the source, while dehydration melting generates granitic liquids [53]. However, there are different opinions on the genetic mode or tectonic

setting of TTGs. Two main but different views have been proposed: (1) Partial melting genesis of mafic material underplated beneath thickened crust [54–56]; (2) partial melting of the subduction oceanic crust [6] (for example, the subduction of young oceanic crust, the subduction initiation, and ridge subduction [57]). The Phanerozoic TTGs were similar to adakites known to be formed in subduction environments and were in association with fore-arc basalts (FABs), boninites (high-Mg andesite), and Nb-enriched basalts/Nb-enriched gabbros [7,48].

It is generally believed that Phanerozoic TTG rocks are sodic rocks formed in the island arc environment of the ocean subduction zone [1,2,4,7,36]. In the Rb-(Y + Nb) and Rb-(Yb + TA) diagrams (Figure 8a,b [6,48,58–60]), the Gaolihan trondhjemite fell within the field of volcanic arc granites, indicating an island arc environment [61,62]. In the Rb-(Y + Nb) and Rb-(Yb + TA) diagrams (Figure 8c), the samples plotted mainly in the TTG area and all five fell within the field of adakite and TTG, reflecting an island arc environment of the ocean subduction zone. In the (Th/Yb)-Nb/Yb diagram (Figure 8d), the samples fell in the overlapping area of an oceanic island arc and continental arc. All these diagrams indicated that the Gaolihan trondhjemite formed in the island arc environment of the oceanic subduction zone.

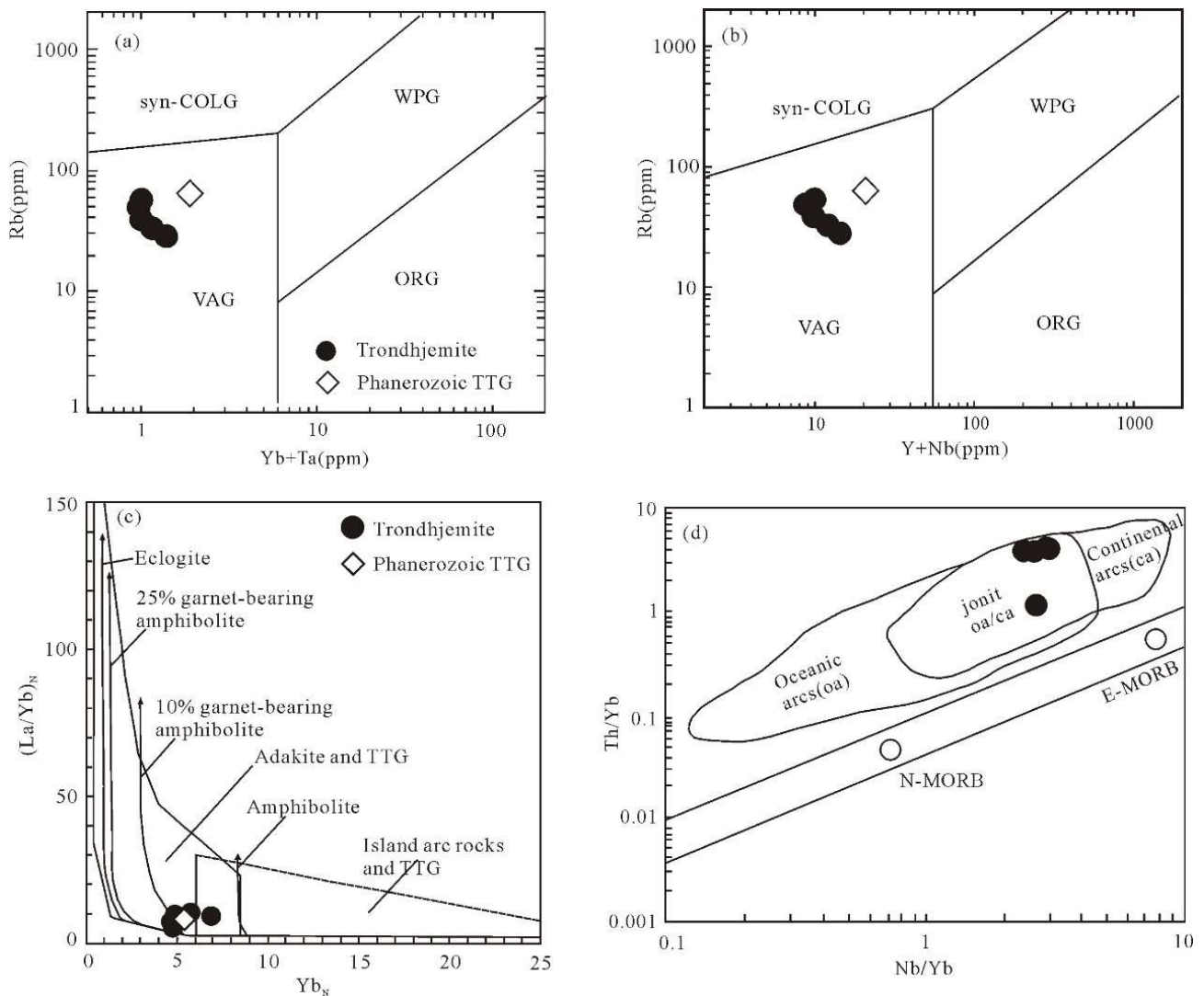


Figure 8. Rb vs. (Yb + Ta) diagram [58] (a), Rb vs. (Y + Nb) diagram [58] (b), (La/Yb)_N vs. Yb_N diagram [48,59] (c), and (Th/Yb) vs. (La/Yb) vs. Th diagram [60] (d) of the Gaolihan trondhjemite. Phanerozoic TTG data from Condie, 2005 [6].

The experimental results showed that TTG-like felsic melts can be produced only when free water is available in the source, “however free water is only available in the case of subducted slab melting, thus leading to the genesis of trondhjemites” [53,63]. All these arguments suggest that TTGs are generated in a subduction-related geodynamic setting.

The Gaolihan trondhjemite was characterized by typical geochemical characteristics formed in an island arc of the suprasubduction zone; were consistent with the fore-arc basalts, boninites, and adakites in the Early Carboniferous Diyanmiao ophiolite; and composed a relatively complete (intra-oceanic) arc igneous rock structural assemblage [21] (Figures 1 and 2), indicating the trondhjemite represented a partial melting of a subducted oceanic slab.

The characteristics of subducted oceanic basalts are Na-rich, K-poor, and high $\text{Na}_2\text{O}/\text{K}_2\text{O}$ values. In addition, the Gaolihan trondhjemite had a higher content of Si and $\text{Mg}^\#$ (Table 1). It is generally believed that the $\text{Mg}^\#$ of the partial melting of basalts is less than 45, while the TTG melt formed by the melting of oceanic subduction plates needs to pass through mantle wedge peridotite in the process of rising to the surface and must interact with the mantle wedge peridotite. This interaction will increase the $\text{Mg}^\#$ of the residual melt [4]. Therefore, the Gaolihan trondhjemite may be the TTG melt formed by the partial melting of the subduction oceanic crust, which interacted with the mantle wedge peridotite in the process of rising to the surface through the subduction zone.

6.2. Tectonic Implications of the Trondhjemite: Constraints of Intra-Oceanic Subduction in the Southern Paleo-Asian Ocean

TTG occurs throughout geologic time and has contributed to the growth of continental crust [56]. It is crucial to understand the source and origin of TTGs to better understand the formation and tectonic evolution of continental crust [56]. Many scientists believe that intra-oceanic arcs are important sites of juvenile continental crust formation and that the subduction-related TTG-type granitoid magmatism is a main contributor to continental growth [7]. As one of the typical igneous rock assemblages formed in the island arc environment, Phanerozoic TTGs are combined with island arc magmatic rocks such as fore-arc basalt, high magnesium andesite (boninite)/high magnesium diorite, magnesium andesite, adakite, and Nb-enriched gabbro basalt/gabbro, and are important petrological records of oceanic subduction and Cenozoic arc crustal growth events [1,7,64].

The Hegenshan suture zone, which is located in the southeastern CAOB (Figure 1b), carries numerous ophiolite slices and island arc magmatic rocks. Safonova [7] reported on intra-oceanic arcs and TTGs in the CAOB and considered that TTG magmatism in intra-oceanic and continental margin arcs is an important geological process for the growth of new continental crust. Therefore, the recognition of the Diyanmiao primary arc igneous rock association may reveal that the Paleo-Asian Ocean was still in the stage of (intra-oceanic) oceanic crust subduction, intra oceanic arc TTG magmatism, and neocontinental crust growth in the Late Carboniferous. Şengör et al. [64] proposed that the CAOB was mainly formed as a subduction-related accretionary complex and magmatic arc and considered that the continental crust was accretionary mainly through tectonic accretion along the oceanic subduction zone (forming a subduction accretionary complex) and emplacement of Cenozoic magmatic rocks (forming a magmatic arc). The authors of [64] pointed out that the Paleo-Asian Ocean finally closed along the Solonker suture zone in the Triassic. The island-arc-type TTG in the Late Carboniferous oceanic subduction zone reported in this paper formed a relatively complete structural combination of primary arc igneous rocks with the Early Carboniferous Diyanmiao SSZ ophiolite (harzburgite and layered-massive gabbro), forearc basalt (FAB), boninite, and adakite (granodiorite) [21,30], creating the Early Carboniferous–Late Carboniferous Diyanmiao ophiolite-TTG rock belt. The identification of island arc TTGs in the oceanic subduction zone in the Late Carboniferous (309.2 ± 2.1 Ma) indicated that the Paleo-Asian Ocean was in the stage of oceanic subduction and juvenile continental crust formation in the Late Carboniferous.

The zircon U-Pb age of 309.2 ± 2.1 Ma obtained for the Gaolihan trondhjemite coincided with the formation age of Late Carboniferous island arc magmatic rocks in central Inner Mongolia combined with the Early Carboniferous Diyanmiao ophiolite (~340 Ma) [30], fore-arc basalt (335.6 Ma), boninite (~328 Ma) [21], and Late Carboniferous adakite (315 Ma) [47] identified in central Inner Mongolia in recent years, which further supported the interpretation that the southern PAO had not closed by the Late Carboniferous but was undergoing intra-oceanic subduction. In other words, the Late Carboniferous recorded the initial stages of subduction of the Diyanmiao intra-oceanic arc within the southern PAO, with subsequent subduction of oceanic crust. Combined with the studies on the initial subduction in the ocean, the characteristic lithological assemblage of an intra-oceanic forearc of the initial subduction in the ocean in the eastern part of the Paleo-Asian Ocean from the Early Carboniferous to Late Carboniferous can be preliminarily established: SSZ-type ophiolite (serpentinized harzburgite and layered-massive gabbro), fore-arc basalt (FAB), boninite, and adakite TTGs. Based on our field observations, a geochemical data analysis of the Diyanmiao ophiolite and TTGs, and a comparison of the IBM initial subduction system [37], we inferred a subduction initiation model in the Diyanmiao intra-oceanic arc during the Early Carboniferous to the Late Carboniferous. The Early Carboniferous intra-oceanic subduction initiation in the southeast of the Paleo-Asian Ocean began along a transform fault or fault zone [32] (Figure 9a). After the initial sinking of the slab, asthenospheric upwelling and decompression melting [65] led to forearc spreading and the formation of Diyanmiao FABs (335.6 Ma) (Figure 9b) [21,32]. The Diyanmiao FABs represented the initial subduction stage. Asthenospheric upwelling and decompression melting [66] following the initial sinking of the slab resulted in forearc spreading and formation of the Diyanmiao FABs (335.6 Ma) (Figure 9b). As the subduction initiation process continued, leading to further decompression melting, boninites (328 Ma) were generated at this stage (Figure 9c). The newly discovered trondhjemite (309 Ma) may represent the partial melting of the subducted oceanic crust at a greater depth (Figure 9d). The above information revealed that the initial subduction of the initial intra-oceanic may have occurred in the eastern part of the Paleo-Asian Ocean from the Early Carboniferous to the Late Carboniferous.

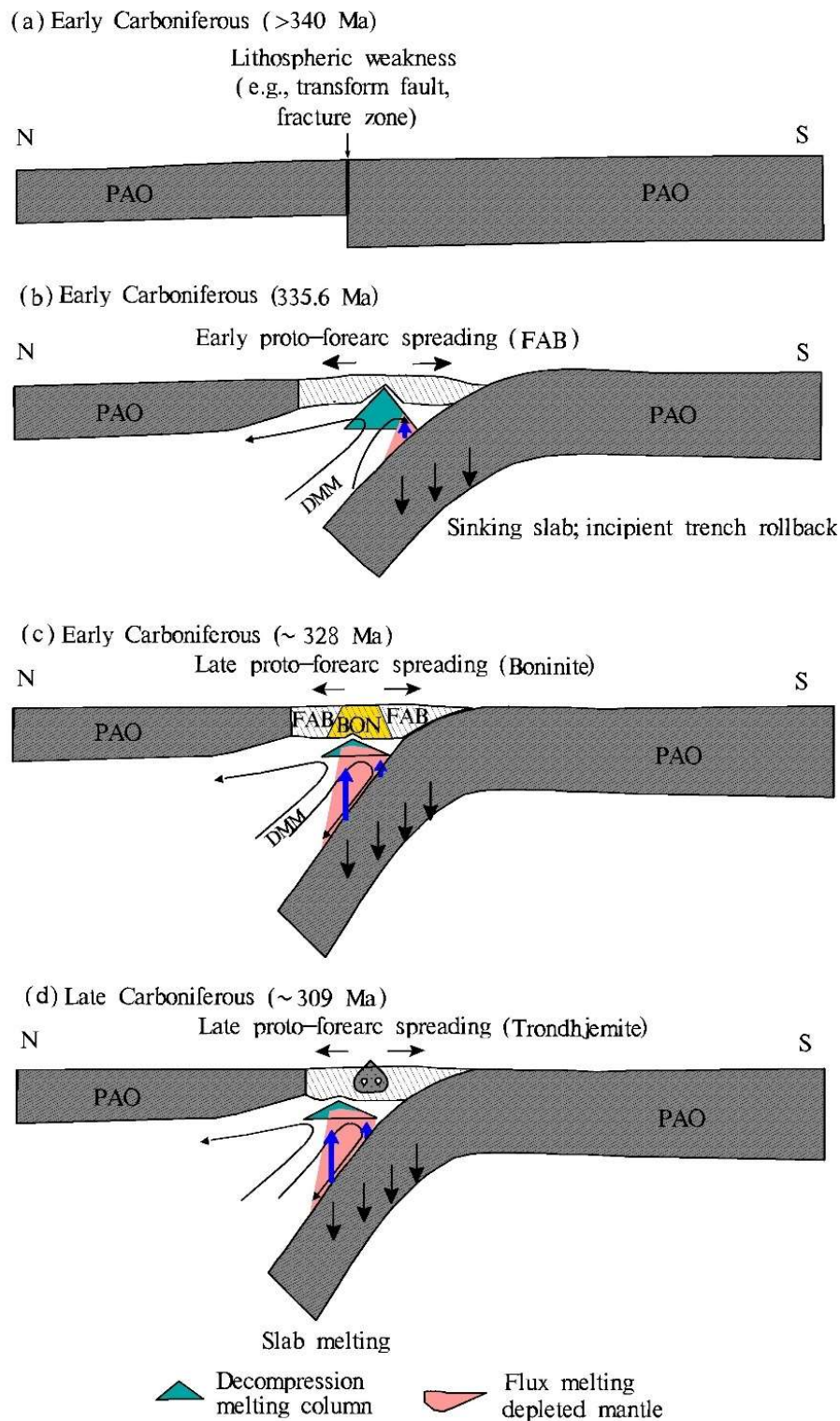


Figure 9. Evolution of the early Carboniferous to late Carboniferous Diyanmiao intra-oceanic forearc system in central Inner Mongolia as based on the subduction infancy model [21,32,65,67,68]. (a) Oceanic crust boundary preceding subduction initiation. (b) Early Carboniferous subduction initiation, leading to forearc spreading and formation of FABs. (c) As the subduction initiation process continued, boninites were formed. (d) As the subduction process continued, the oceanic crust partially melts at a deeper depth, trondhjemite were form. DMM is depleted MORB mantle. FAB—forearc basalt. PAO—Paleo-Asian Ocean.

7. Conclusions

- (1) The petrological and geochemical characteristics indicated that the Gaolihan trondhjemite belonged to the tonalite–trondhjemite–granodiorite (TTG) series and formed via melting of the subducted oceanic crust.
- (2) The Gaolihan trondhjemite crystallized at 309.2 ± 2.1 Ma, reflecting the subduction-related TTG-type granitoid magmatism and indicating that the southern Paleo-Asian Ocean was in the process of subduction, TTG magmatism, and juvenile continental crust formation in the Late Carboniferous.

Author Contributions: Conceptualization, P.D. and Y.L.; methodology, P.D., Y.L., H.L., and J.W.; software, P.D. and Y.L.; validation, P.D. and Y.L.; formal analysis, P.D.; investigation, P.D., Y.L., and J.W.; resources, P.D. and Y.L.; data curation, P.D. and Y.L.; writing—original draft preparation, P.D. and Y.L.; writing—review and editing, P.D., Y.L., Y.X., H.L., and J.W.; visualization, P.D.; supervision, P.D.; project administration, Y.L.; funding acquisition, Y.L. All authors have read and agreed to the published version of the manuscript.

Funding: This research was funded by the National Natural Science Foundation of China (grant/award number: 41972061), the China Geological Survey (grant/award number: 1212011120711), and the Science and Technology Innovation Team Program of Hebei GEO University (KJCXTD-2021-07).

Data Availability Statement: The data presented in this study are available upon request from the corresponding author.

Conflicts of Interest: The authors declare no conflict of interest.

References

1. Foley, S.F.; Buhre, S.; Jacob, D.E. Evolution of the Archaean crust by delamination and shallow subduction. *Nature* **2003**, *421*, 249–252. [[CrossRef](#)]
2. Rapp, R.P.; Shimizu, N.; Norman, M.D. Growth of early continental crust by partial melting of eclogite. *Nature* **2003**, *425*, 605–609. [[CrossRef](#)] [[PubMed](#)]
3. Foley, S.F.; Tiepolo, M.; Vannucci, R. Growth of early continental crust controlled by melting of amphibolite in subduction zones. *Nature* **2002**, *417*, 837–840. [[CrossRef](#)] [[PubMed](#)]
4. Rapp, R.P.; Watson, E.B. Dehydration melting of metabasalt at 8–32 kbar: Implications for continental growth and crust mantle recycling. *J. Petrol.* **1995**, *36*, 891–931. [[CrossRef](#)]
5. Martin, H.; Smithies, R.H.; Rapp, R.; Moyen, J.F. An overview of adakite, tonalite-trondhjemite-granodiorite (TTG), and sanukitoid: Relationships and some implications for crustal evolution. *Lithos* **2005**, *79*, 1–24. [[CrossRef](#)]
6. Condie, K.C. TTGs and adakites: Are they both slab melts? *Lithos* **2005**, *80*, 33–44. [[CrossRef](#)]
7. Safonova, I. Juvenile versus recycled crust in the Central Asian Orogenic belt: Implications from ocean plate stratigraphy, blueschist belts and intra-oceanic arcs. *Gondwana Res.* **2017**, *47*, 6–27. [[CrossRef](#)]
8. Dobretsov, N.L.; Buslov, M.M.; Vernikovskiy, V.A. Neoproterozoic to Early Ordovician Evolution of the Paleo-Asian Ocean: Implications to the Break-up of Rodinia. *Gondwana Res.* **2003**, *6*, 143–159. [[CrossRef](#)]
9. Khain, E.V.; Bibikova, E.V.; Salnikova, E.B.; Kröner, A.; Gibsher, A.S.; Didenko, A.N.; Degtyarev, K.E.; Fedotova, A.A. The Palaeo-Asian ocean in the Neoproterozoic and early Palaeozoic: New geochronologic data and palaeotectonic reconstructions. *Precambrian Res.* **2003**, *122*, 329–358. [[CrossRef](#)]
10. Filippova, I.B.; Bush, V.A.; Didenko, A.N. Middle Paleozoic subduction belts: The leading factor in the formation of the Central Asian fold-and-thrust belt. *Rus. J. Earth Sci.* **2002**, *3*, 405–426. [[CrossRef](#)]
11. De Jong, K.; Xiao, W.J.; Windley, B.F.; Masago, H.; Lo, C.H. Ordovician $40\text{Ar}/39\text{Ar}$ phengite ages from the blueschist-facies Ondor Sum subduction-accretion complex (Inner Mongolia) and implications for the early Paleozoic history of continental blocks in China and adjacent areas. *Am. J. Sci.* **2006**, *306*, 799–845. [[CrossRef](#)]
12. Wilhem, C.; Windley, B.F.; Stampfli, G.M. The Altaids of Central Asia: A tectonic and evolutionary innovative review. *Earth Sci. Rev.* **2012**, *113*, 303–341. [[CrossRef](#)]
13. Eizenhöfer, P.R.; Zhao, G.; Zhang, J.; Sun, M. Final closure of the Paleo-Asian Ocean along the Solonker Suture Zone: Constraints from geochronological and geochemical data of Permian volcanic and sedimentary rocks. *Tectonics* **2014**, *33*, 441–463. [[CrossRef](#)]
14. Kröner, A. The Central Asian Orogenic Belt—Present knowledge and comparison with the SW Pacific. In *The Central Asian Orogenic Belt—Geology, Evolution, Tectonics, and Models. Contributions to the Regional Geology of the Earth*; Kröner, A., Ed.; Borntraeger Science Publishers: Stuttgart, Germany, 2015; p. 313.
15. Xiao, W.; Windley, B.F.; Sun, S.; Li, J.; Huang, B.; Han, C.; Yuan, C.; Sun, M.; Chen, H. A Tale of Amalgamation of Three Permo-Triassic Collage Systems in Central Asia: Oroclines, Sutures, and Terminal Accretion. *Ann. Rev. Earth Planet. Sci.* **2015**, *43*, 477–507. [[CrossRef](#)]

16. Jahn, B.M.; Windley, B.; Natal'in, B.; Dobretsov, N. Phanerozoic continental growth in Central Asia. *J. Asian Earth Sci.* **2004**, *23*, 599–603. [[CrossRef](#)]
17. Li, J.Y. Permian geodynamic setting of Northeast China and adjacent regions: Closure of the Paleo-Asian Ocean and subduction of the Paleo-Pacific Plate. *J. Asian Earth Sci.* **2006**, *26*, 207–224. [[CrossRef](#)]
18. Xiao, W.J.; Windley, B.F.; Huang, B.C.; Han, C.M.; Yuan, C.; Chen, H.L.; Li, J.L. End-Permian to mid-Triassic termination of the accretionary processes of the southern Altai: Implications for the geodynamic evolution, Phanerozoic continental growth, and metallogeny of Central Asia. *Int. J. Earth Sci.* **2009**, *98*, 1189–1217. [[CrossRef](#)]
19. Windley, B.F.; Alexeiev, D.; Xiao, W.L.; Kröner, A.; Badarch, G. Tectonic models for accretion of the Central Asian Orogenic Belt. *J. Geol. Soc.* **2007**, *164*, 31–47. [[CrossRef](#)]
20. Xiao, W.J.; Song, D.F.; Windley, B.F.; Li, J.L.; Han, C.M.; Wan, B.; Zhang, J.E.; Ao, S.J.; Zhang, Z.Y. Research progresses of the accretionary processes and metallogenesis of the Central Asian Orogenic Belt. *Sci. China Earth Sci.* **2019**, *49*, 1512–1545, (In Chinese with English Abstract).
21. Li, Y.J.; Wang, G.H.; Santosh, M.; Wang, J.F.; Li, H.Y. Subduction initiation of the SE Paleo-Asian Ocean: Evidence from a well preserved intra-oceanic forearc ophiolite fragment in central Inner Mongolia. *Earth Planet. Sci. Lett.* **2020**, *535*, 116087. [[CrossRef](#)]
22. Xiao, W.J.; Windley, B.F.; Hao, J.; Zhai, M.G. Accretion leading to collision and the Permian Solonker suture, Inner Mongolia, China: Termination of the central Asian orogenic belt. *Tectonics* **2003**, *22*, 1069. [[CrossRef](#)]
23. Jian, P.; Liu, D.Y.; Kröner, A.; Windley, B.F.; Shi, Y.R.; Zhang, W.; Zhang, F.Q.; Miao, L.C.; Zhang, L.Q.; Tomurhuu, D. Evolution of a Permian intraoceanic arc-trench system in the Solonker suture zone, Central Asian Orogenic Belt, China and Mongolia. *Lithos* **2010**, *118*, 169–190. [[CrossRef](#)]
24. Xu, B.; Charvet, J.; Chen, Y.; Zhao, P.; Shi, G.Z. Middle Paleozoic convergent orogenic belts in western Inner Mongolia (China): Framework, kinematics geochronology and implications for tectonic evolution of the Central Asian Orogenic Belt. *Gondwana Res.* **2013**, *23*, 1342–1364. [[CrossRef](#)]
25. Reagan, M.K.; Ishizuka, O.; Stern, R.J.; Kelley, K.A.; Ohara, Y.; Blichert-Toft, J.; Bloomer, S.H.; Cash, J.; Fryer, P.; Hanan, B.B.; et al. Fore-arc basalts and subduction initiation in the Izu-Bonin-Mariana system. *Geochem. Geophys. Geosyst.* **2010**, *11*, Q03X12. [[CrossRef](#)]
26. Wang, Q.; Liu, X.Y. Paleoplate tectonics between Cathaysia and Angara in Inner Mongolia of China. *Tectonics* **1986**, *5*, 1073–1088. [[CrossRef](#)]
27. Song, S.G.; Wang, M.M.; Xu, X.; Wang, C.; Niu, Y.; Allen, M.B.; Su, L. Ophiolites in the Xing'an-Inner Mongolia accretionary belt of the CAO: Implications for two cycles of seafloor spreading and accretionary orogenic events. *Tectonics* **2015**, *34*, 2221–2248. [[CrossRef](#)]
28. Nozaka, T.; Liu, Y. Petrology of the Hegenshan ophiolite and its implications for the tectonic evolution of northern China. *Earth Planet. Sci. Lett.* **2002**, *202*, 89–104. [[CrossRef](#)]
29. Robinson, P.T.; Bai, W.J.; Yang, J.S.; Hu, X.F.; Zhou, M.F. Geochemical constraints on petrogenesis and crustal accretion of the Hegenshan ophiolite, northern China. *Acta Petrol. Sin.* **1995**, *11*, 112–124, (In Chinese with English Abstract).
30. Li, Y.J.; Wang, G.H.; Santosh, M.; Wang, J.F.; Dong, P.P.; Li, H.Y. Suprasubduction zone ophiolites from Inner Mongolia, North China: Implications for the tectonic history of the southeastern Central Asian Orogenic Belt. *Gondwana Res.* **2018**, *59*, 126–143. [[CrossRef](#)]
31. Li, Y.J.; Wang, J.F.; Li, H.Y.; Dong, P.P. Recognition of Meilaotewula ophiolite in Xi U jimqin Banner, Inner Mongolia. *Acta Petrol. Sin.* **2015**, *31*, 1461–1470, (In Chinese with English Abstract).
32. Li, Y.J.; Wang, J.F.; Xin, H.T.; Dong, P.P. Subduction initiation in the southeastern Palaeo-Asian Ocean: Constraints from early Permian adakites in suprasubduction zone ophiolites, central Inner Mongolia, North China. *Geol. J.* **2020**, *55*, 2044–2061. [[CrossRef](#)]
33. Eizenhöfer, P.R.; Zhao, G.; Sun, M.; Zhang, J.; Han, Y.G.; Hou, W. Geochronological and Hf isotopic variability of detrital zircons in Paleozoic strata across the accretionary collision zone between the North China craton and Mongolian arcs and tectonic implications. *Geol. Soc. Am. Bull.* **2015**, *127*, 1422–1436. [[CrossRef](#)]
34. Jian, P.; Kröner, A.; Windley, B.F.; Shi, Y.R.; Zhang, W.; Zhang, L.Q.; Yange, W.R. Carboniferous and Cretaceous mafic-ultramafic massifs in Inner Mongolia (China): A SHRIMP zircon and geochemical study of the previously presumed integral "Hegenshan ophiolite". *Lithos* **2012**, *142–143*, 48–66. [[CrossRef](#)]
35. Wang, S.Q.; Hu, X.J.; Yang, Z.L.; Zhao, H.L.; Zhang, Y.; Hao, S.; He, L. Geochronology, Geochemistry, Sr-Nd-Hf Isotopic Characteristics and Geological Significance of Carboniferous Yuejin Arc Intrusive Rocks of Xilinhot, Inner Mongolia. *Earth Sci.* **2018**, *43*, 1–31.
36. Xue, J.P.; Liu, M.Y.; Li, G.Z.; Zhao, G.M. Zircon geochronology and geochemistry of Haer Bogetuoer TTG rock, Solonker zone, Inner Mongolia and their tectonic implications. *Earth Sci. Front.* **2018**, *25*, 230–239.
37. Ishizuka, O.; Tani, K.; Reagan, M.K. Izu-Bonin-Mariana forearc crust as a modern ophiolite analogue. *Elements* **2014**, *10*, 115–120. [[CrossRef](#)]
38. Liu, Y.S.; Gao, S.; Hu, Z.C.; Gao, C.G.; Zong, K.Q.; Wang, D.B. Continental and oceanic crust recycling-induced melt-peridotite interactions in the Trans-North China Orogen: U-Pb dating, Hf isotopes and trace elements in zircons of mantle xenoliths. *J. Petrol.* **2010**, *51*, 537–571. [[CrossRef](#)]

39. Ludwig, K.R. *ISOPLOT 3.00: A Geochronological Toolkit for Microsoft Excel*; Berkeley Geochronology Center: Berkeley, CA, USA, 2003; 39p.
40. Fan, Y.X. The composition and evolution of the late Paleozoic inner-oceanic arc in Xiwuqi, Inner Mongolia. *Chin. Acad. Geol. Sci.* **2019**, *1*, 1–137.
41. Wang, J.F.; Li, Y.J.; Li, H.Y.; Dong, P.P. Discovery of the Late Carboniferous adakite in the Erenhot-Hegenshan suture zone and intra-oceanic subduction of the Paleo-Asian Ocean. *Geol. China* **2021**, *48*, 520–535, (In Chinese with English Abstract).
42. Bach, W.; Alt, J.C.; Niu, Y.L.; Humphris, S.E.; Erzinger, J.; Dick, H.J. The geochemical consequences of late-stage low-grade alteration of lower ocean crust at the SW Indian Ridge: Results from ODP Hole 735B (Leg 176). *Geochim. Cosmochim. Acta* **2001**, *65*, 3267–3287. [[CrossRef](#)]
43. O'Connor, J.T. A classification for quartz-rich igneous rocks based on feldspar ratios. *U.S. Geol. Surv. Prof. Pap.* **1965**, *525-B*, 79–84.
44. Barker, F.; Arth, J.G. Generation of trondhjemitic-tonalitic liquids and Archaean bimodal trondhjemite-basalt suites. *Geology* **1976**, *4*, 596–600. [[CrossRef](#)]
45. Le Bas, M.J.; Maiter, R.W.; Streckeisen, A.; Zanettin, B. A chemical classification of volcanic rocks based on the total alkali-silica diagram. *J. Petrol.* **1986**, *27*, 745–750. [[CrossRef](#)]
46. Peccerillo, A.; Taylor, S.R. Geochemistry of Eocene calc-alkaline volcanic rocks from the Kastamonu area, northern Turkey. *Contrib. Mineral. Petrol.* **1976**, *58*, 63–81. [[CrossRef](#)]
47. Sun, S.S.; McDonough, W.F. Chemical and isotopic systematics of oceanic basalts: Implications for mantle composition and processes. In *Magmatism in the Ocean Basins*; Saunders, A.D., Norry, M.J., Eds.; Geological Society of London, Special Publication: London, UK, 1989; Volume 42, pp. 313–345.
48. Wang, S.; Li, Y.J.; Wang, J.F.; Dong, P.P.; Li, H.Y.; Guo, L.L.; Wang, X.C. Discovery of Late Carboniferous adakite in Manita, Inner Mongolia, and its constrains on intra-oceanic subduction in eastern Paleo-Asian Ocean. *Geol. Bull. China* **2021**, *40*, 82–94, (In Chinese with English Abstract).
49. Defant, M.J.; Drummond, M.S. Derivation of some modern arc magmas by melting of young subducted lithosphere. *Nature* **1990**, *347*, 662–665. [[CrossRef](#)]
50. Kelemen, P.B.; Hangh, K.; Ureenem, A.R. One view of the geochemistry of subduction-related magmatic arcs, with an emphasis on primitive andesite and lower crust. In *Treatise on Geochemistry*; Rudnick, R.L., Ed.; Elsevier: Amsterdam, The Netherlands, 2003; Volume 3, pp. 593–659.
51. Hoskin, P.W.O.; Schaltegger, U. The composition of zircon and igneous and metamorphic petrogenesis. *Rev. Mineral. Geochem.* **2003**, *53*, 27–62. [[CrossRef](#)]
52. Azizi, H.; Zanjefili Beiranvand, M.; Asahara, Y. Zircon U-Pb ages and petrogenesis of a tonalite-trondhjemite-granodiorite (TTG) complex in the northern Sanandaj-Sirjan Zone, northwest Iran: Evidence for Late Jurassic arc-continent collision. *Lithos* **2014**, *216–217*, 178–195. [[CrossRef](#)]
53. Prouteau, G.; Scaillet, B.; Pichavant, M.; Maury, R.C. Evidence for mantle metasomatism by hydrous silicic melts derived from subducted oceanic crust. *Nature* **2001**, *410*, 197–200. [[CrossRef](#)] [[PubMed](#)]
54. Rudnick, R.L. Making continental crust. *Nature* **1995**, *378*, 571–577. [[CrossRef](#)]
55. Albare' de, F. The growth of continental crust. *Tectonophysics* **1998**, *296*, 1–14. [[CrossRef](#)]
56. Smithies, R.H. The Archaean tonalite-trondhjemite-granodiorite (TTG) series is not an anologue of Cenozoic adakite. *Earth Planet. Sci. Lett.* **2000**, *182*, 115–125. [[CrossRef](#)]
57. Gutscher, M.A.; Spakman, W.; Bijward, H.; Engdahl, E.R. Geodynamics of flat subduction: Seismicity and tomographic evidence from the Andean margin. *Tectonics* **2000**, *19*, 814–833. [[CrossRef](#)]
58. Pearce, J.A.; Lippard, S.J.; Roberts, S. Characteristics and tectonic significance of supra-subduction zone ophiolites. In *Marginal Basin Geology*; Kokelaar, B.P., Howells, M.F., Eds.; Geological Society of London, Special Publication: London, UK, 1984; Volume 16, pp. 77–94.
59. Martin, H. Adakitic magmas: Modern analogues of Archaean granitoids. *Lithos* **1999**, *46*, 411–429. [[CrossRef](#)]
60. Pearce, J.A.; Peate, D.W. Tectonic implications of the composition of volcanic arc magma. *Ann. Rev. Earth Planet. Sci.* **1995**, *23*, 251–285. [[CrossRef](#)]
61. Thorkelson, D.J.; Breitsprecher, K. Partial melting of slab window margins: Genesis of adakitic and non-adakitic magmas. *Lithos* **2005**, *79*, 24–41. [[CrossRef](#)]
62. Viruete, J.E.; Contreras, F.; Stein, C. Magmatic relationships and ages between adakites, magnesian andesites and Nb-enriched basalt-andesites from Hipaniola: Record of a major change in the Caribbean island arc magma sources. *Lithos* **2007**, *99*, 151–177. [[CrossRef](#)]
63. Martin, H.; Moyen, J.F. Secular changes in tonalite-trondhjemite-granodiorite composition as markers of the progressive cooling of Earth. *Geology* **2002**, *30*, 319–322. [[CrossRef](#)]
64. Şengör, A.M.C.; Natalin, B.A.; Burtman, V.S. Evolution of the Altaid tectonic collage and Paleozoic crustal growth in Eurasia. *Nature* **1993**, *364*, 299–307. [[CrossRef](#)]
65. Reagan, M.K.; Pearce, J.A.; Petronotis, K.; Almeev, R.; Avery, A.J.; Carvallo, C.; Whattam, S.A. Subduction initiation and ophiolite crust: New insights from IODP drilling. *Int. Geol. Rev.* **2017**, *59*, 1439–1450. [[CrossRef](#)]
66. Stern, R.J.; Gerya, T. Subduction initiation in nature and models: A review. *Tectonophysics* **2018**, *746*, 173–198. [[CrossRef](#)]

-
67. Li, H.Y.; Taylor, R.N.; Prytulak, J.; Kirchenbaur, M.; Shervais, J.W.; Ryan, J.G.; Godard, M.; Reagan, M.K.; Pearce, J.A. Radiogenic isotopes document the start of subduction in the Western Pacific. *Earth Planet. Sci. Lett.* **2019**, *518*, 197–210. [[CrossRef](#)]
 68. Whattam, S.A.; Stern, R.J. The 'subduction initiation rule': A key for linking ophiolites, intra-oceanic forearcs, and subduction initiation. *Contribut. Mineral. Petrol.* **2011**, *162*, 1031–1045. [[CrossRef](#)]